High-dose sodium propionate contributes to tumor immune escape through the IGF2BP3/PD-L1 axis in colorectal cancer

XUN WANG[1] and YIKUI HU[2]

[1]Department of Gastroenterology, Wuhan Wuchang Hospital, Wuchang Hospital Affiliated to Wuhan University of Science and Technology, Wuhan, Hubei 430063, P.R. China; [2]Department of Neurology, Wuhan Wuchang Hospital, Wuchang Hospital Affiliated to Wuhan University of Science and Technology, Wuhan, Hubei 430063, P.R. China

Received August 15, 2024; Accepted March 20, 2025

DOI: 10.3892/ol.2025.15049

Abstract. The understanding of how gut microbiota metabolites modulate immune escape mechanisms in colorectal cancer (CRC) remains limited. In the present study, the impact of gut microbiota metabolites on the efficacy of programmed cell death protein 1 (PD-1) and programmed cell death ligand-1 (PD-L1) immunotherapy in CRC was explored, with a particular focus on the short-chain fatty acid, sodium propionate (SP), as they key metabolite. The results of the present study, determined by CCK-8 and flow cytometry, demonstrated that 10 mM SP significantly suppressed CRC cell proliferation and induced apoptosis. By contrast, 40 mM SP, but not 10 mM, markedly increased the PD-L1 mRNA and protein expression levels. Insulin-like growth factor 2 mRNA binding protein 3 (IGF2BP3) expression, analyzed via bioinformatics using The Cancer Genoma Atlas datasets, was significantly higher in CRC tissues compared with healthy tissues. Additionally, survival analysis uncovered that elevated IGF2BP3 levels in tumor tissues were strongly associated with poor clinical outcomes. Moreover, 40 mM SP significantly induced the expression of IGF2BP3 mRNA and protein in CRC cells. The actinomycin D assay was conducted to assess mRNA stability, whereas methylated RNA immunoprecipitation coupled with quantitative polymerase chain reaction (qPCR) and RNA immunoprecipitation-qPCR were utilized to confirm the interaction between IGF2BP3 and PD-L1 mRNA. These results indicated that IGF2BP3 served as an N6-methyladenosine (m6A) reader for PD-L1, stabilizing its mRNA in an m6A-dependent manner, thereby upregulating the PD-L1 mRNA and protein expression levels. Therefore, high-dose SP may promote tumor immune escape via the IGF2BP3/PD-L1 axis in CRC. As such, high-dose SP may synergize with PD-1/PD-L1 blockade therapies to improve clinical outcomes in patients with CRC, particularly by upregulating PD-L1 expression.

Correspondence to: Dr Yikui Hu, Department of Neurology, Wuhan Wuchang Hospital, Wuchang Hospital Affiliated to Wuhan University of Science and Technology, 116 Yangyuan Street, Wuchang, Wuhan, Hubei 430063, P.R. China
E-mail: huyikui202404@126.com

Key words: colorectal cancer, insulin-like growth factor 2 mRNA binding protein 3, immune escape, programmed cell death ligand-1, sodium propionate

Introduction

Colorectal cancer (CRC) is the third most common cancer worldwide (1), with patients frequently experiencing poor prognoses primarily due to acquired drug resistance and mechanisms underlying immune escape (2,3). The programmed cell death protein 1 (PD-1)/programmed cell death ligand-1 (PD-L1) signaling axis is a vital pathway that facilitates tumor immune escape (4), where tumor cells expressing PD-L1 interact with PD-1 on T cells. The identification of small molecule drugs that improve the efficacy of PD-1/PD-L1 immunotherapy is critical for enhancing CRC treatment outcomes.

There has been growing interest in investigating the impact of intestinal microbiota and its metabolites on host immunity (5,6). Among these metabolites, short-chain fatty acids (SCFAs), such as acetate, propionate and butyrate, are produced through the microbial fermentation of dietary carbohydrates in the gut (7). SCFAs are central to maintaining normal gastrointestinal functions, such as immune modulation and host metabolism (8,9). SCFAs exhibit protective effects by modulating the inflammatory cascade, including the inhibition of the nuclear factor-κB and histone deacetylase pathways (10,11). Acetate is the most abundant SCFA and accounts for ~50% of all SCFAs in the colon (12). Researchers have elucidated its potential role in cancer immunotherapy. For example, Tran *et al* (13) reported that acetate reduced the expression of poliovirus receptor/cluster of differentiation (CD)155 in colorectal cancer cells, thus upregulating $CD8^+$ T cell activity against cancer. Peng *et al* (14) demonstrated that gut microbiota that produced SCFAs were positively associated with an anti-PD-1/PD-L1 response in gastrointestinal malignancies. These findings highlight the role of SCFAs in resisting tumor immune escape. Certain reports have described the role and molecular mechanisms underlying sodium propionate (SP) in cancer progression. For instance, Park *et al* (15) reported that SP suppressed breast cancer cell proliferation and induced cell apoptosis in tumor-bearing mice

in vivo via the Janus kinase 2/signal transducer and activator of transcription 3/reactive oxygen species/p38 mitogen-activated protein kinase pathway. Kim *et al* (16) demonstrated that SP promoted apoptosis and induced cell cycle arrest in lung cancer. However, the role and mechanisms underlying SP in CRC remain unclear.

Understanding the interplay between drug resistance and immune escape mechanisms is vital, particularly since prolonged or high-dose drug treatments may promote drug resistance through pathways linked to immune evasion (17,18). Tsai *et al* (19) reported that cisplatin upregulated PD-L1 expression in bladder cancer by targeting the extracellular signal-regulated protein kinase 1/2 and activator protein-1 pathways, indicating that the immune escape mechanism may induce chemoresistance. Additionally, cisplatin has been shown to enhance PD-L1 expression in non-small cell lung cancer, and its combined use with PD-1/PD-L1 pathway inhibitors increased treatment efficacy in tumor-bearing models *in vivo* (20).

The present study aimed to explore the effects of high-dose SP on PD-L1 expression in CRC cells and to investigate the underlying mechanisms to identify novel therapeutic strategies for overcoming immune escape in CRC.

Materials and methods

Cell culture and transfection. The HCT116 and SW480 cell lines were acquired from Procell Life Science & Technology Co., Ltd. and cultured in Dulbecco's Modified Eagle Medium (Thermo Fisher Scientific, Inc.). The medium was supplemented with 10% fetal bovine serum (Thermo Fisher Scientific, Inc.) and 1% penicillin/streptomycin solution (Beijing Solarbio Science & Technology Co., Ltd.). The cells were maintained in a humidified incubator at 37˚C with 5% CO_2. For the transfections, the short hairpin (sh)RNA and negative control (NC) scrambled shRNA sequences were inserted into the pLKO.1 plasmid (MilliporeSigma), resulting in the formation of pLKO.1-shRNA and pLKO.1-sh-NC constructs. The targeting portions of the sequence in sh-IGF2BP3#1, sh-IGF2BP3#2, sh-IGF2BP3#3 and sh-NC were as follows: sh-IGF2BP3#1, 5'-GGTGCTGGATAGTTTACTA-3'; sh-IGF2BP3#2, 5'-GGTAAAGCAGCACCAACAA-3'; sh-IGF2BP3#3, 5'-CGATGTCCACCGTAAAGAA-3'; and sh-NC: 5'-CAACAAGATGAAGAGCACCAA-3'. For the transfection, 2 μg of pLKO.1-shRNA or pLKO.1-sh-NC plasmid DNA was diluted in 250 μl Opti-MEM medium (Thermo Fisher Scientific, Inc.), mixed with 5 μl Lipofectamine® 2000 reagent (pre-diluted in 250 μl Opti-MEM) and incubated at room temperature for 20 min to form transfection complexes. The complexes were added to cells and incubated at 37˚C with 5% CO_2 for 6 h, after which the medium was replaced with fresh complete medium. Cells were harvested 48 h post-transfection for subsequent functional or molecular analyses.

Cell Counting Kit-8 (CCK-8) assay. A commercial CCK-8 (Beijing Solarbio Science & Technology Co., Ltd.) was used for this assay. First, the half-maximal inhibitory concentration (IC_{50}) of SP was determined using the CCK-8 assay. For this, HCT116 cells were seeded into 96-well plates and treated with SP at gradient concentrations of 0.16, 0.8, 4, 20, 100 and 500 mM for 48 h at 37˚C. After treatment, 10 μl CCK-8 reagent was added to each well and incubated with the HCT116 cells for 2 h. Finally, the optical density (OD) at 450 nm was recorded. Second, to analyze cell viability, HCT116 and SW480 cells were seeded into 96-well plates and treated with 10 mM SP for 48 h. Consequently, 10 μl CCK-8 reagent was added to the cells and incubated for 2 h. The OD at 450 nm was again detected.

Immunofluorescence (IF) assay. The abundance of proliferating cell nuclear antigen (PCNA) in CRC cells was analyzed by an IF assay. After SP treatment, the cells were fixed with 4% paraformaldehyde at room temperature (25˚C) for 20 min, permeabilized with 0.1% Triton X-100 in Tris-buffered saline and blocked with 3% donkey serum (MilliporeSigma) at 25˚C for 1 h. Subsequently, the cells were incubated with an anti-PCNA antibody (cat no. GB11010; 1:500; Wuhan Servicebio Technology Co., Ltd.) diluted in blocking buffer at 4˚C overnight, followed by incubation with Alexa Fluor 488-conjugated goat anti-mouse IgG secondary antibody (cat no. GB25301; 1:800; Wuhan Servicebio Technology Co., Ltd.) at 25˚C for 1 h in the dark. The nuclei were then stained using 4',6-diamidino-2-phenylindole (DAPI; MilliporeSigma; 1 μg/ml) at 25˚C for 10 min. Fluorescence images were captured under a Zeiss LSM 900 confocal microscope (Carl Zeiss AG), with a scale bar of 100 μm. Fluorescence intensity quantification was performed with ImageJ software (version 1.53; National Institutes of Health).

Flow cytometry. Cell apoptosis was analyzed using flow cytometry. First, CRC cells were seeded into 6-well plates and treated with 10 mM SP for 48 h. Second, the cells were harvested, washed three times with ice-cold PBS and resuspended in ice-cold phosphate-buffered saline. Third, the cells were stained with 50 μg/ml annexin V-fluorescein isothiocyanate (BD Biosciences) and 10 μg/ml propidium iodide (BD Biosciences) in the dark for 15 min. Finally, the cells were analyzed using a FACSCalibur flow cytometer (BD Biosciences), and the apoptosis rate was analyzed using FlowJo software (version 10.8.1; FlowJo LLC; BD Biosciences).

Reverse transcription-quantitative polymerase chain reaction (RT-qPCR). Total RNA samples were extracted from the CRC cells using the EastepTM Universal RNA Extraction Kit (Promega Corporation), and cDNA was synthesized using the GoScriptTM Reverse Transcription System (Promega Corporation). The kit was used according to the manufacturer's instructions. qPCRs were conducted using the GoTaq® qPCR Master Mix (Promega Corporation) on the ABI 7500 Fast Real-Time PCR System (Applied Biosystems; Thermo Fisher Scientific, Inc.) under the following thermocycling conditions: Initial denaturation at 95˚C for 2 min; 40 cycles of denaturation at 95˚C for 15 sec and annealing/extension at 60˚C for 30 sec. Glyceraldehyde-3-phosphate dehydrogenase (GAPDH), the housekeeping gene, served as the internal control. Relative gene expression was analyzed by the $2^{-\Delta\Delta Cq}$ method (21). The primer sequences for PD-L1, IGF2BP3 and GAPDH were as follows: PD-L1 forward primer (F), 5'-GGTAGAGTATGGTAGCAATATG-3'; PD-L1 reverse primer (R), 5'-CCTTCAGGTCTTCCTCTCCA-3'; IGF2BP3 F, 5'-TTC

AAGGACGCCAAGATCCC-3'; IGF2BP3 R, 5'-TCCCAC TGTAAATGAGGCGG-3'; GAPDH F, 5'-GTCAAGGCT GAGAACGGGAA-3'; and GAPDH R, 5'-AAATGAGCCCCA GCCTTCTC-3'.

Western blot assay. The CRC cells were harvested, washed with PBS and lysed in ice-cold radioimmunoprecipitation assay buffer (Beyotime Institute of Biotechnology) for 30 min on ice. Then, protein concentrations were measured using the bicinchoninic acid protein assay kit (Pierce; Thermo Fisher Scientific, Inc.). The protein samples (35 μg/lane) were then separated by 12% sodium dodecyl sulfate-polyacrylamide gel electrophoresis and transferred to polyvinylidene difluoride membranes. The membranes were blocked with 5% skimmed milk at room temperature for 1 h and then incubated overnight with the following primary antibodies at 4˚C overnight: anti-PD-L1 (cat. no. GB11339A; 1:5,000; Wuhan Servicebio Technology Co., Ltd.), anti-IGF2BP3 (cat. no. 14642-1-AP; 1:5,000; Proteintech Group, Inc.) and anti-GAPDH (cat. no. GB15002; 1:20,000; Wuhan Servicebio Technology Co., Ltd.). The next day, the membranes were incubated with a horseradish peroxidase-conjugated secondary antibody (cat. no. GB23303/GB23301; 1:20,000; Wuhan Servicebio Technology Co., Ltd.) at 25˚C for 1 h. Finally, the immunoreactive protein bands were visualized using an enhanced chemiluminescence kit (Beyotime Institute of Biotechnology). Densitometry was conducted using ImageJ software (version 1.53; National Institutes of Health), with GAPDH as the internal reference.

Bioinformatics analysis. The m6A2Target database (http://m6a2target.canceromics.org) was used to predict N6-methyladenosine (m6A) modification-associated proteins upstream of PD-L1. Genes co-expressed with PD-L1 were analyzed using the R package ggplot2 (version 3.3.6; https://cran.r-project.org/package=ggplot2). IGF2BP3 expression data in colon adenocarcinoma (COAD) and rectum adenocarcinoma (READ) tissues, along with their corresponding healthy tissues, were downloaded from The Cancer Genome Atlas (TCGA, https://portal.gdc.cancer.gov/) and compared using the Wilcoxon signed-rank test using R statistical software (version 4.2.1; https://www.r-project.org/). PD-L1 expression data were downloaded from COAD and READ datasets in TCGA. Kaplan-Meier survival curves was first constructed to visualize the association between survival outcomes and pathological grades. The log-rank test was then performed using R statistical software (version 4.2.1; https://www.r-project.org/).

Actinomycin D (ActD) assay. The stability of PD-L1 mRNA was analyzed using the ActD assay. After transfection with sh-NC or sh-IGF2BP3#2 for 48 h, 2 μg/ml of the transcription inhibitor, ActD (MilliporeSigma), was added to the wells. After ActD exposure for 0, 1, 2 or 4 h at 37˚C, the cells were harvested and PD-L1 expression was measured by RT-qPCR.

Methylated RNA immunoprecipitation (meRIP)-qPCR assay. The meRIP-qPCR assay was conducted as described previously (22). To inhibit m^{6}A methylation, HCT116 cells were treated with 100 μM S-adenosylhomocysteine (SAH) dissolved in serum-free DMEM for 48 h at 37˚C. Control cells were incubated with an equal volume of solvent (0.1% DMSO in serum-free DMEM) under identical conditions. Total RNA was extracted from HCT116 cells using TRIzol® Reagent (Invitrogen; Thermo Fisher Scientific, Inc.) and treated with DNase I (Thermo Fisher Scientific Inc.) based on the manufacturer's instructions. RNA (10 μg) was fragmented in 10 mM $ZnCl_2$ at 94˚C for 5 min, followed by incubation with mouse anti-m6A monoclonal antibodies diluted at a 1:300 ratio, labeled Protein G Dynabeads (cat. no. 10003D; Thermo Fisher Scientific, Inc.) at a ratio of 5 μg antibody per 1 mg Dynabeads at 4˚C for 2 h. A 50 μl volume of conjugated Dynabeads slurry was added to each RNA sample. After incubation, beads were washed three times with high-salt buffer (50 mM Tris-HCl pH 7.4, 1 M NaCl, 1% NP-40) and once with low-salt buffer (50 mM Tris-HCl pH 7.4, 0.1 M NaCl). Beads were separated using a magnetic stand and bound RNA was eluted in Elution Buffer (10 mM Tris-HCl pH 7.0, 1 mM EDTA, 0.5% SDS) at 65˚C for 10 min. qPCR was performed using SYBR Green Master Mix (Takara Bio, Inc.) on the ABI 7500 Fast Real-Time PCR System (Applied Biosystems; Thermo Fisher Scientific, Inc.), following the aforementioned protocol. The normalization was performed using the 'Input' fraction. The PD-L1 primers used in the RIP-qPCR assay were as follows: PD-L1 F, 5'-CCCATACAACAAAATCAACCAAAG-3'; and PD-L1 R: 5'-CTTGGAATTGGTGGTGGTGGTC-3'.

RIP-qPCR assay. The interaction between IGF2BP3 protein and PD-L1 mRNA was confirmed using a RIP assay as described previously (23). Cells were lysed in RIPA buffer (Thermo Fisher Scientific, Inc.). For each IP reaction, 500 μg of lysate was incubated with 5 μg of anti-IGF2BP3 antibodies, diluted at a 1:200 ratio (cat. no. 14642-1-AP; Proteintech Group, Inc.) and 50 μl Protein G magnetic beads (Thermo Fisher Scientific, Inc.) at 4˚C overnight. Beads were washed three times with high-salt wash buffer (500 mM NaCl, 0.1% NP-40, 50 mM Tris-HCl, pH 7.4) and once with low-salt buffer (150 mM NaCl, 0.1% NP-40, 50 mM Tris-HCl, pH 7.4), with each wash step involving centrifugation at 3,000 x g for 5 min at 4˚C. RNA was isolated from the immunoprecipitated complexes using TRIzol® reagent (Invitrogen; Thermo Fisher Scientific, Inc.) and quantified by qPCR as aforementioned.

Statistical analysis. All experiments were conducted in triplicate. Data were analyzed using GraphPad Prism 8.0 software (Dotmatics), with the results expressed as the mean ± SD. The unpaired student's t-test was conducted to compare the differences between two groups. One-way analysis of variance followed by Tukey's test was used to compare among multiple groups. $P<0.05$ was considered to indicate a statistically significant difference.

Results

Low-dose SP restrains CRC cell proliferation and triggers cell apoptosis in vitro. The effects of SP on the biological behavior of CRC cells was assessed through a series of functional experiments. The IC_{50} value of SP in the HCT116 cell line was 10.39 mM (Fig. 1A). Subsequently, 10 mM SP was selected for further assays. SP treatment markedly reduced CRC cell

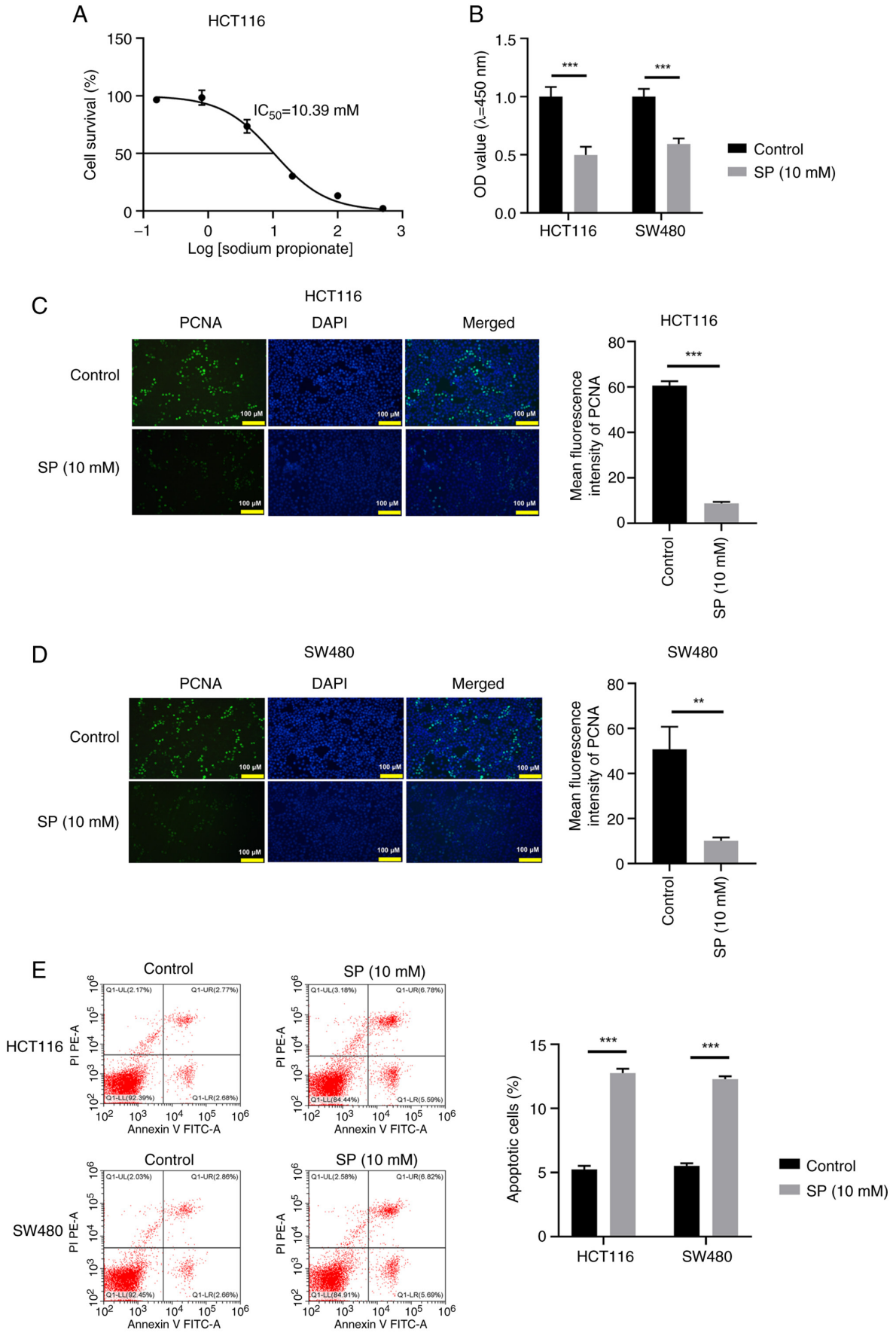

Figure 1. Low-dose SP restrains colorectal cancer cell proliferation and triggers cell apoptosis *in vitro*. (A) IC_{50} value of SP in HCT116 cells was determined by CCK-8 assay. HCT116 and SW480 cells were then exposed to 10 mM SP for 48 h. (B) CCK-8 assay was implemented to analyze cell viability. Immunofluorescence assay was performed to analyze the abundance of PCNA in the (C) HCT116 and (D) SW480 cell lines. (E) Flow cytometry was conducted to examine the cell apoptotic rate. $^{**}P<0.01$, $^{***}P<0.001$. SP, sodium propionate; IC_{50}, half-maximal inhibitory concentration; CCK-8, Cell Counting Kit-8; PCNA, proliferating cell nuclear antigen; OD, optical density.

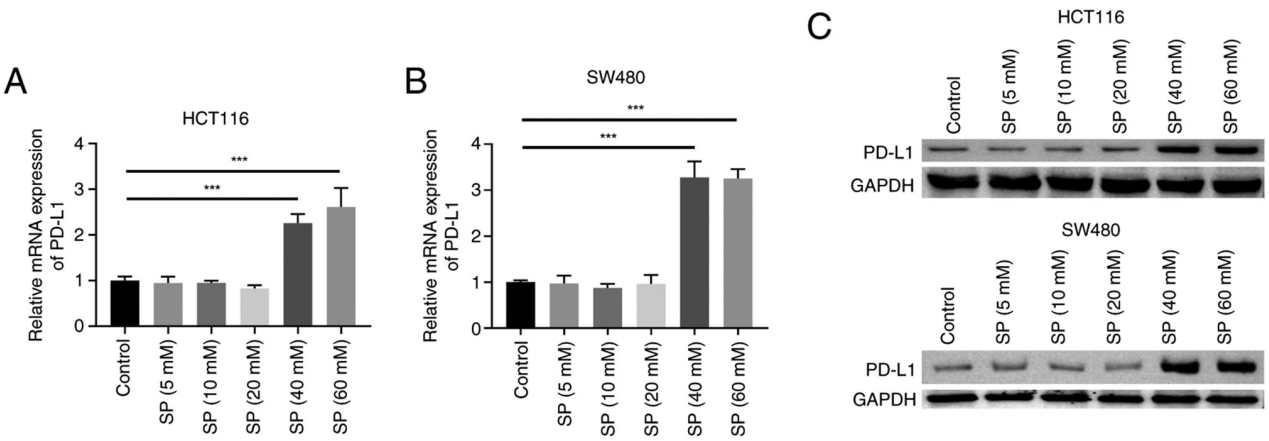

Figure 2. High-dose SP induces the expression of PD-L1 in CRC cells. CRC cells were treated with gradient concentrations of SP (5, 10, 20, 40 and 60 mM) for 48 h, and the (A and B) mRNA and (C) protein expression of PD-L1 was determined by reverse transcription-quantitative polymerase chain reaction and western blotting in HCT116 and SW480 cells. ***P<0.001. SP, sodium propionate; PD-L1, programmed cell death ligand-1; CRC, colorectal cancer; GAPDH, glyceraldehyde-3-phosphate dehydrogenase.

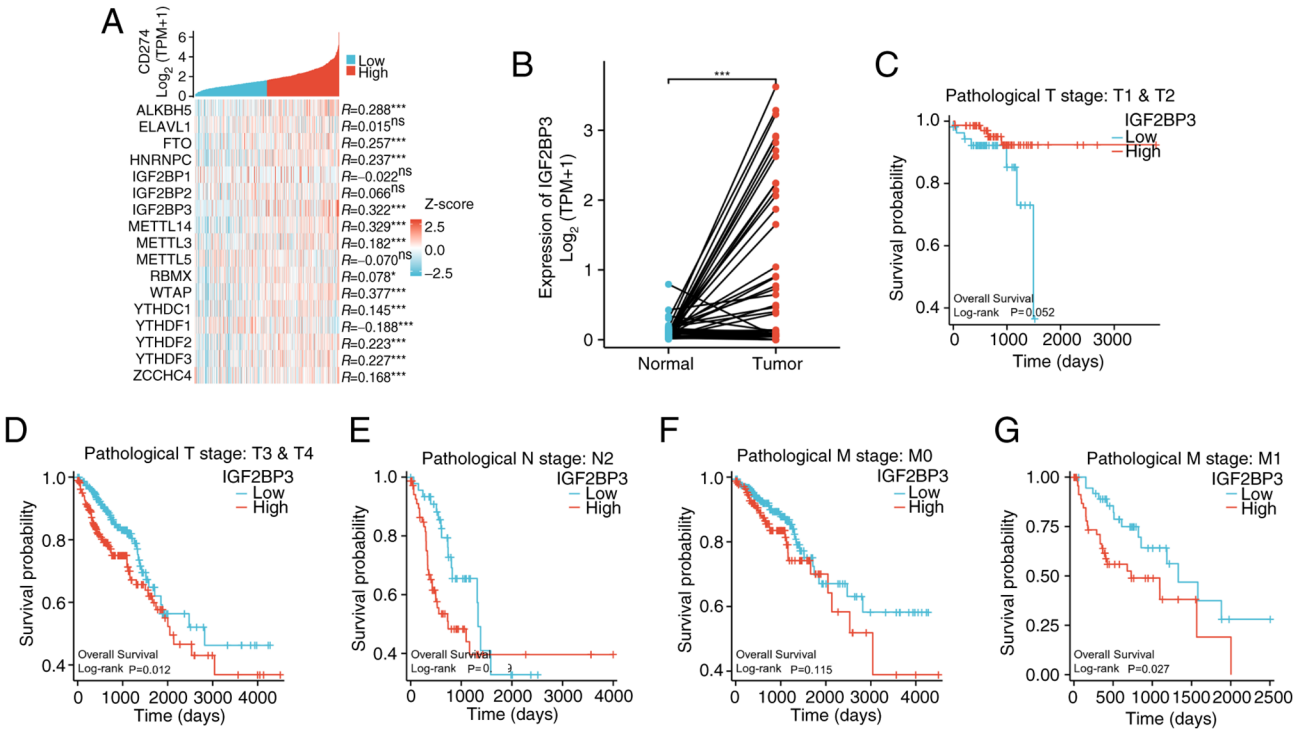

Figure 3. Screening for potential upstream molecules mediating PD-L1 expression regulation. (A) Genes with similar expression pattern to PD-L1 were analyzed by R package ggplot2 (v3.3.6). (B) The expression of IGF2BP3 in COAD and READ tissues along with their paired normal tissues in TCGA database was analyzed by Wilcoxon signed-rank test. (C-G) The PD-L1 expression data was downloaded from the COAD and READ datasets in TCGA database, and the associations between survival and different pathological grades were analyzed by log-rank test. *P<0.05, ***P<0.001. ns, not statistically significant; PD-L1, programmed cell death ligand-1; COAD, colon adenocarcinoma; READ, rectum adenocarcinoma; TCGA, The Cancer Genome Atlas; TPM, transcripts per million; T, tumor; N, node; M, metastasis.

viability (Fig. 1B). PCNA, a marker of cell proliferation, was identified using the IF assay, which indicated a notable reduction in PCNA abundance after SP treatment (Fig. 1C and D). Additionally, SP treatment triggered apoptosis in CRC cells (Fig. 1E). Taken together, 10 mM SP exerted an antitumor effect on CRC cells.

High-dose SP induces PD-L1 expression in CRC cells. Acquired drug resistance in tumor cells has been strongly associated with immune escape (24). PD-L1 is a pivotal mediator of T cell activity, and the PD-L1/PD-1 pathway mediates tumor immune escape (25). In the present study, the effects of different doses of SP on PD-L1 expression in CRC cells were investigated. SP (5, 10 and 20 mM) exerted marginal effects on the PD-L1 mRNA and protein expression levels in the HCT116 and SW480 cell lines. By contrast, SP (40 and 60 mM) significantly induced PD-L1 mRNA and protein expression compared with the control group (Fig. 2).

Table I. N6-methyladenosine-associated proteins upstream of programmed cell death ligand-1 in *Homo sapiens*, as predicted by the m6A2Target database.

RM2Target ID	WERs name	WERs type	Target gene
RM2Target_629483	ALKBH5	Eraser	CD274
RM2Target_629484	ALKBH5	Eraser	CD274
RM2Target_629485	ALKBH5	Eraser	CD274
RM2Target_629486	ALKBH5	Eraser	CD274
RM2Target_795954	ELAVL1	Reader	CD274
RM2Target_795955	ELAVL1	Reader	CD274
RM2Target_690420	FTO	Eraser	CD274
RM2Target_690418	FTO	Eraser	CD274
RM2Target_690416	FTO	Eraser	CD274
RM2Target_690417	FTO	Eraser	CD274
RM2Target_690419	FTO	Eraser	CD274
RM2Target_875022	HNRNPC	Reader	CD274
RM2Target_905481	IGF2BP1	Reader	CD274
RM2Target_905482	IGF2BP1	Reader	CD274
RM2Target_905483	IGF2BP1	Reader	CD274
RM2Target_905484	IGF2BP1	Reader	CD274
RM2Target_969166	IGF2BP2	Reader	CD274
RM2Target_983717	IGF2BP3	Reader	CD274
RM2Target_174114	METTL14	Writer	CD274
RM2Target_174111	METTL14	Writer	CD274
RM2Target_174112	METTL14	Writer	CD274
RM2Target_174113	METTL14	Writer	CD274
RM2Target_268126	METTL3	Writer	CD274
RM2Target_268130	METTL3	Writer	CD274
RM2Target_268131	METTL3	Writer	CD274
RM2Target_268127	METTL3	Writer	CD274
RM2Target_268123	METTL3	Writer	CD274
RM2Target_268124	METTL3	Writer	CD274
RM2Target_268125	METTL3	Writer	CD274
RM2Target_268128	METTL3	Writer	CD274
RM2Target_268129	METTL3	Writer	CD274
RM2Target_268132	METTL3	Writer	CD274
RM2Target_390715	METTL5	Writer	CD274
RM2Target_1026942	RBMX	Reader	CD274
RM2Target_562730	WTAP	Writer	CD274
RM2Target_562729	WTAP	Writer	CD274
RM2Target_562728	WTAP	Writer	CD274
RM2Target_1102913	YTHDC1	Reader	CD274
RM2Target_1102912	YTHDC1	Reader	CD274
RM2Target_1141739	YTHDF1	Reader	CD274
RM2Target_1141737	YTHDF1	Reader	CD274
RM2Target_1141736	YTHDF1	Reader	CD274
RM2Target_1141738	YTHDF1	Reader	CD274
RM2Target_1181191	YTHDF2	Reader	CD274
RM2Target_1181189	YTHDF2	Reader	CD274
RM2Target_1181190	YTHDF2	Reader	CD274
RM2Target_1181188	YTHDF2	Reader	CD274
RM2Target_1233355	YTHDF3	Reader	CD274
RM2Target_611035	ZCCHC4	Writer	CD274

WERs, writers, erasers and readers.

Table II. Validation and contextual information of predicted m6A-associated proteins interacting with PD-L1 in various cell lines, as identified by the m6A2Target database.

RM2Target ID	Cell line	Validated	Binding	Perturbation	Confidence	Motif
RM2Target_629483	THP1	-	-	44595	2	44638
RM2Target_629484	HCCC9810	1	-	-	1	44638
RM2Target_629485	RBE	1	-	-	1	44638
RM2Target_629486	MOLM13	-	-	44562	1	44638
RM2Target_795954	THP1	-	44562	44562	2	44758
RM2Target_795955	T24	-	44562	-	1	44758
RM2Target_690420	HCT116	1	-	-	1	44731
RM2Target_690418	HeLa	-	44562	-	1	44731
RM2Target_690416	253J	-	-	44562	1	44731
RM2Target_690417	NB4	-	-	44562	1	44731
RM2Target_690419	Huh7	-	-	44562	1	44731
RM2Target_875022	MCF7	-	-	44562	1	44852
RM2Target_905481	ES2	-	-	44594	2	44728
RM2Target_905482	MV3	-	-	44594	2	44728
RM2Target_905483	K562	-	44562	-	1	44728
RM2Target_905484	SK-N-AS	-	-	44562	1	44728
RM2Target_969166	J82	-	-	44562	1	44669
RM2Target_983717	PL45	-	44562	-	1	44729
RM2Target_174114	HEK293T	-	44562	44595	3	44578
RM2Target_174111	A549	-	-	44562	1	44578
RM2Target_174112	HSC3	-	-	44562	1	44578
RM2Target_174113	IMR-90	-	-	44562	1	44578
RM2Target_268126	HeLa	-	44564	44598	3	44669
RM2Target_268130	HEK293T	-	44563	44596	3	44669
RM2Target_268131	LNCaP	-	-	44595	2	44669
RM2Target_268127	SCC9	1	-	-	1	44669
RM2Target_268123	HUVEC	-	-	44562	1	44669
RM2Target_268124	DKO-1	-	-	44562	1	44669
RM2Target_268125	EndoC-βH1	-	-	44562	1	44669
RM2Target_268128	U2OS	-	-	44562	1	44669
RM2Target_268129	HEC-1A	-	-	44563	1	44669
RM2Target_268132	HEL	-	-	44562	1	44669
RM2Target_390715	HeLa	-	-	44563	1	44700
RM2Target_1026942	HEK293T	-	44563	-	1	44729
RM2Target_562730	HEL	-	-	44594	2	44574
RM2Target_562729	HeLa	-	44564	-	1	44574
RM2Target_562728	MDA-LM2	-	-	44562	1	44574
RM2Target_1102913	HeLa	-	44562	-	1	44632
RM2Target_1102912	MOLM13	-	-	44563	1	44632
RM2Target_1141739	PC9	1	-	-	1	44633
RM2Target_1141737	A549	-	44562	-	1	44633
RM2Target_1141736	A172	-	-	44562	1	44633
RM2Target_1141738	AGS	-	-	44562	1	44633
RM2Target_1181191	PC9	1	-	-	1	44758
RM2Target_1181189	H1299	-	44562	-	1	44758
RM2Target_1181190	GSC11	-	44562	-	1	44758
RM2Target_1181188	HeLa	-	-	44564	1	44758
RM2Target_1233355	MDA-MB-231	-	44562	-	1	44664
RM2Target_611035	HepG2					

Validated, whether the interaction between the m6A-associated protein and PD-L1 has been experimentally validated (1 for validated, '-' for not validated). Binding, shows if there is evidence of direct binding between the protein and its target RNA, as supported by specific assays or databases (a unique identifier or '-' if not available). Perturbation, indicates whether perturbation experiments (e.g., knockdown or overexpression) have demonstrated effects on the target gene expression (a unique identifier or '-' if not available). Confidence, represents the confidence level of the predicted interaction, with higher numbers indicating stronger or more reliable predictions. Motif, refers to the specific nucleotide sequence or structural motif that the m6A-associated protein recognizes or binds to on the RNA.

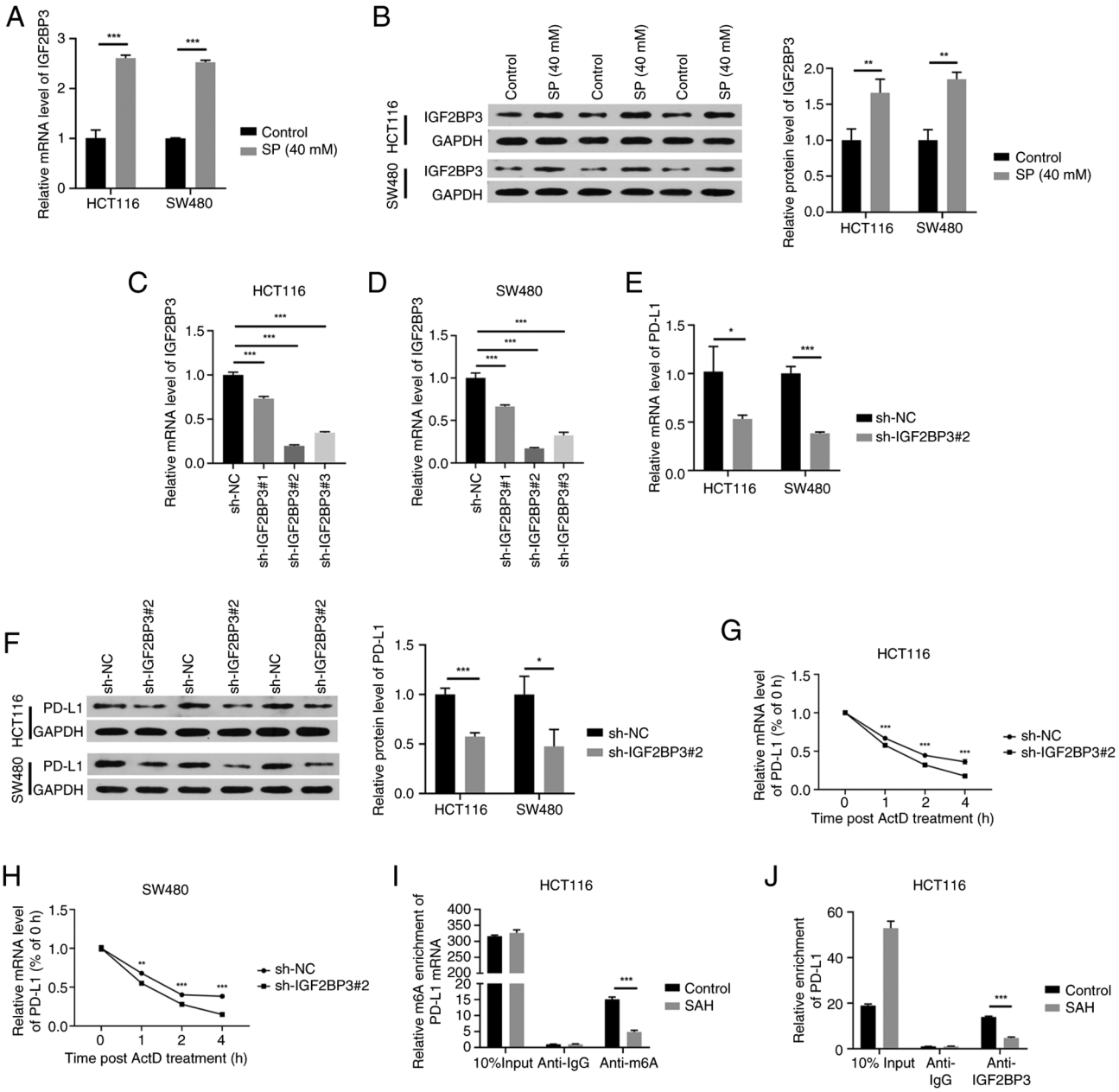

Figure 4. m6A 'reader' IGF2BP3 enhances PD-L1 mRNA stability in an m6A-dependent manner. (A) RT-qPCR and (B) western blotting were performed to detect the mRNA and protein expression, respectively, of IGF2BP3 in CRC cells upon SP exposure (40 mM for 48 h). The interference efficiencies of three IGF2BP3 shRNAs (sh-IGF2BP3#1, sh-IGF2BP3#2 and sh-IGF2BP3#3) in (C) HCT116 and (D) SW480 cells were evaluated by RT-qPCR. CRC cells were transfected with sh-NC or sh-IGF2BP3#2 and the (E) mRNA and (F) protein levels of PD-L1 were determined by RT-qPCR and western blotting, respectively. The stability of PD-L1 mRNA upon IGF2BP3 knockdown in (G) HCT116 and (H) SW480 cells was analyzed by adding ActD. (I) Methylated RIP-qPCR was performed to measure m6A modification level of PD-L1 mRNA upon the addition of SAH. (J) RIP-qPCR was implemented to test the interaction between IGF2BP3 and PD-L1 upon the addition of SAH. *P<0.05, **P<0.01, ***P<0.001. CRC, colorectal cancer; IGF2BP3, insulin-like growth factor 2 mRNA binding protein 3; PD-L1, programmed cell death ligand-1; SP, sodium propionate; shRNA, short hairpin RNA; NC, negative control; RT-qPCR, reverse transcription-quantitative polymerase chain reaction; ActD, actinomycin D; SAH, S-adenosylhomocysteine; RIP, RNA immunoprecipitation; m6A, N6-methyladenosine; GAPDH, glyceraldehyde-3-phosphate dehydrogenase.

Additionally, 40 and 60 mM SP exhibited comparable effects on promoting PD-L1 mRNA and protein expression. Although 5, 10 and 20 mM SP could inhibit cell viability, only 40 and 60 mM SP could promote PD-L1 expression. Therefore, relative to the 5, 10 and 20 mM doses, the SP dose that could enhance PD-L1 expression (40 mM) was defined as the 'high' dose. Considering that for most 'cold' tumors, tumor cell expression of PD-L1 is a prerequisite for PD-1/PD-L1 immunotherapy, the present study focused more on the mechanisms by which high dose SP (40 mM) regulated PD-L1 expression, to explore new ways to enhance the sensitivity of PD-1/PD-L1 immunotherapy.

Screening for potential upstream molecules that mediate PD-L1 expression. The present study explored whether m6A modification mediated the SP-induced aberrant upregulation of PD-L1. Predictions using the m6A2Target database identified 17 candidate m6A-associated proteins

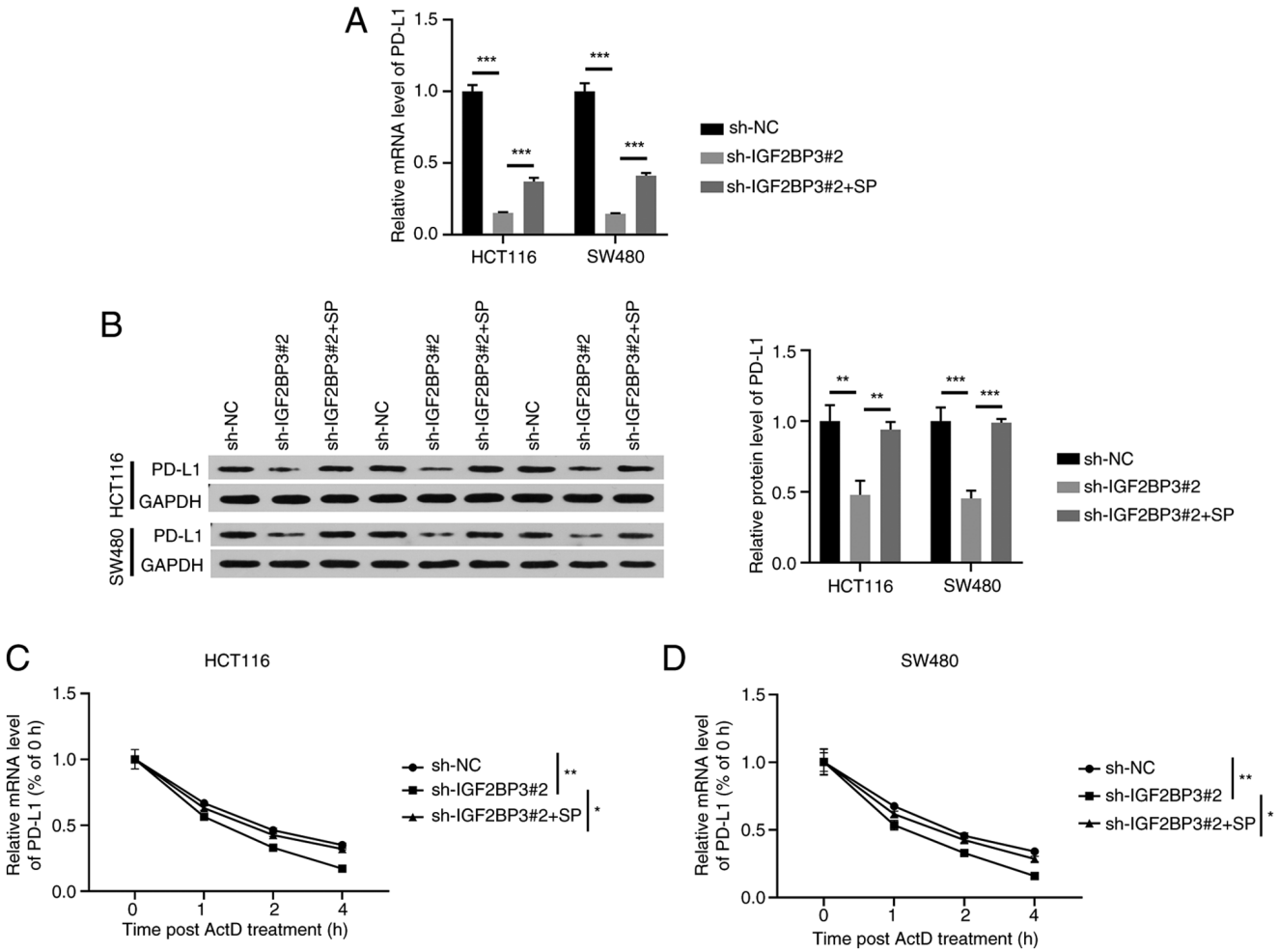

Figure 5. IGF2BP3 mediates SP-induced stabilization of PD-L1 mRNA in CRC cells. HCT116 and SW480 cells were treated with sh-NC, sh-IGF2BP3#2 or sh-IGF2BP3#2 + SP and (A) reverse transcription-quantitative polymerase chain reaction and (B) western blotting were implemented to determine the mRNA and protein expression of PD-L1 in CRC cells. The stability of PD-L1 mRNA in treated (C) HCT116 and (D) SW480 cells was analyzed by adding the transcriptional inhibitor, ActD. The significance indicated in the figures pertains to the time point at 4 h. *P<0.05, **P<0.01, ***P<0.001. IGF2BP3, insulin-like growth factor 2 mRNA binding protein 3; PD-L1, programmed cell death ligand-1; SP, sodium propionate; shRNA, short hairpin RNA; NC, negative control; ActD, actinomycin D; GAPDH, glyceraldehyde-3-phosphate dehydrogenase.

upstream of PD-L1 (Tables I and II). Additionally, the R package ggplot2 (v3.3.6) analysis suggested that 12 proteins were positively correlated with PD-L1 (Fig. 3A). Of these, IGF2BP3 was aberrantly upregulated in tumor tissues compared with healthy tissues (Fig. 3B). Additionally, high IGF2BP3 expression was significantly associated with poor prognosis in patients with high-grade tumors (T3/T4, N2 and M1; Fig. 3C-G). Therefore, IGF2BP3 was selected for subsequent analyses.

m6A 'reader' IGF2BP3 enhances PD-L1 mRNA stability in an m6A-dependent manner. First, the effects of SP on IGF2BP3 expression were assessed. Treatment with 40 mM SP significantly upregulated IGF2BP3 mRNA and protein expression in HCT116 and SW480 cells (Fig. 4A and B). IGF2BP3 is an m6A reader and functions by enhancing mRNA stability (26). Subsequently, it was investigated whether IGF2BP3 could stabilize PD-L1 mRNA. ShRNA#2-induced IGF2BP3 knockdown exhibited the highest interference efficiency compared with the sh-NC group (Fig. 4C and D) and was selected for subsequent analyses. IGF2BP3 depletion downregulated PD-L1 mRNA and protein expression in CRC cells (Fig. 4E and F). Furthermore, the addition of ActD suggested that IGF2BP3 knockdown reduced the PD-L1 mRNA stability in HCT116 and SW480 cells (Fig. 4G and H). SAH, a transmethylase inhibitor, reduced m6A modifications of PD-L1 (Fig. 4I). Furthermore, the RIP assay suggested that SAH weakened the interaction between PD-L1 and IGF2BP3 (Fig. 4J). Taken together, the results indicate that SP induces IGF2BP3 expression, stabilizing PD-L1 mRNA in a m6A-dependent manner.

IGF2BP3 mediates SP-induced stabilization of PD-L1 mRNA in CRC cells. Rescue experiments were conducted to further confirm the effects of SP on PD-L1 expression via IGF2BP3. IGF2BP3 knockdown decreased PD-L1 mRNA and protein expression; however, these effects were partly reversed by SP (Fig. 5A and B). Additionally, IGF2BP3 depletion down-regulated the stability of PD-L1 mRNA, whereas SP treatment partly recovered its stability (Fig. 5C and D). Thus, the results indicate that the stabilizing effect of SP on PD-L1 mRNA is dependent on IGF2BP3 activity in CRC cells.

Discussion

SP exerts antitumor effects in multiple malignancies, such as breast cancer (15), lung cancer (16) and CRC (27). Ryu *et al* (27) reported that SP treatment promoted apoptosis in CRC by reducing the expression of protein arginine methyltransferase 1. Similarly, in the present study, 10 mM SP significantly restrained CRC cell proliferation and induced apoptosis.

Cancer cells produce immunosuppressive proteins, leading to the dysfunction and apoptosis of immune cells, thereby promoting immune escape (28). PD-L1, an immunosuppressive protein, interacts with PD-1 expressed on T cells, B cells, dendritic cells and natural killer T cells, and suppresses anticancer immune responses (29). In tumor immunology, tumors are categorized as 'cold' or 'hot' based on their immune microenvironment (30). 'Hot' tumors are characterized by high PD-L1 expression and significant infiltration of effector T lymphocytes along with pro-inflammatory signals, such as interferons and interleukin-2. This immunogenic environment renders 'hot' tumors more responsive to PD-1/PD-L1 checkpoint inhibitors due to their active immune response (31,32). By contrast, 'cold' tumors are characterized by low or no PD-L1 expression along with reduced or absent T-cell infiltration. Poor immune activation leads to weak antitumor immune responses, rendering these tumors less responsive to PD-1/PD-L1 blockade therapies (32). CRC is a common example of a 'cold' tumor and it demonstrates poor sensitivity to immunotherapy. Researchers are focusing on transforming 'cold' tumors into 'hot' tumors to increase the efficacy and response rates of cancer immunotherapy (33). A promising strategy involves upregulating PD-L1 expression and promoting T-cell infiltration within the tumor microenvironment (33). Ubiquitin-specific protease 8 inhibition can enhance the K63-linked ubiquitination of PD-L1 mediated by tumor necrosis factor receptor-associated factor 6 while counteracting its K48-linked ubiquitination; this results in elevated PD-L1 protein expression (34). This regulatory pathway holds promise in reshaping the tumor immune microenvironment to improve the effectiveness of PD-1/PD-L1 blockade therapies. Therefore, the role of high PD-L1 expression in CRC lies in its ability to alter the tumor immune microenvironment from 'cold' to 'hot', improving T cell activity and responsiveness to PD-1/PD-L1 inhibitors. High-dose drugs can induce immune escape-related acquired drug resistance in tumor cells (35). Therefore, the role of high-dose SP on PD-L1 expression in CRC cells was assessed in the present study. High-dose SP (40 mM) significantly upregulated the PD-L1 mRNA and protein expression levels, indicating the implication of SP in PD-L1-mediated immune escape in CRC cells.

m6A methylation is crucial in regulating RNA metabolism, including mRNA splicing, intracellular localization and stability (36). m6A methylation is dynamic and reversible, facilitated by RNA methyltransferases (writers), RNA demethylases (erasers) and m6A reader proteins (36). m6A modification affects tumor onset and progression by regulating the expression of oncogenes and tumor suppressor genes (37). Emerging evidence has suggested that m6A modification plays a significant role in the immune response and tumor microenvironment, influencing cancer immunotherapy effectiveness (38). In the present study, we hypothesized that m6A modification-related proteins mediated the high-dose SP-induced upregulation of PD-L1. In the bioinformatics analysis, the expression pattern of IGF2BP3 was correlated with PD-L1. SP treatment notably upregulated both IGF2BP3 mRNA and protein expression in CRC cells. Additionally, IGF2BP3 positively regulated the PD-L1 mRNA and protein expression levels in CRC cells. Furthermore, the meRIP and RIP assays confirmed IGF2BP3 as an m6A reader for PD-L1. Data from rescue experiments demonstrated that the stabilizing effect of SP on PD-L1 mRNA was dependent on IGF2BP3 activity in CRC cells.

The present study is unique in identifying the specific role of high-dose SP in upregulating the m6A reader, IGF2BP3. This, in turn, stabilizes PD-L1 mRNA and may facilitate immune evasion in CRC. Previous studies have outlined the oncogenic role of IGF2BP3 in CRC. For instance, Chen *et al* (39) illustrated the ability of IGF2BP3 to stabilize EGFR mRNA in an m6A-dependent manner, contributing to cetuximab resistance and CRC progression. In addition, Xu *et al* (40) showed the involvement of IGF2BP3 in promoting aggressive cancer phenotypes in CRC, including enhanced proliferation and migration, which was correlated with poor patient prognosis. Together, these studies established IGF2BP3 as a key factor in CRC oncogenesis. Wan *et al* (41) has elucidated the role of the methyltransferase 3, N6-adenosine-methyltransferase complex catalytic subunit/IGF2BP3 axis in PD-L1 expression in breast cancer, and the present study extends these findings to CRC. By introducing SP as a novel regulatory element in this pathway, the present study adds a new dimension to the understanding of IGF2BP3's role in CRC.

While the present study revealed that high-dose SP enhanced PD-L1 expression by upregulating IGF2BP3 in CRC cells and highlighted the potential of SP combined with PD-1/PD-L1 blockade for CRC treatment, there are several limitations to consider. Primarily, the present study relied heavily on *in vitro* experiments and lacked *in vivo* supporting data. In future studies, we intend to validate the effects of SP and PD-L1 combination therapy in animal models to assess its actual efficacy and safety in a complex biological environment. Additionally, further exploration of the precise molecular interactions between SP, IGF2BP3 and PD-L1 are needed to improve the understanding of their roles in immune regulation and potential influencing factors. These investigations will provide important scientific foundations for the translation of SP and PD-L1 antibody combination therapy strategies into clinical applications.

In conclusion, in the present study, high-dose SP treatment enhanced PD-L1 expression by upregulating IGF2BP3 expression in CRC cells. This finding supports the potential for combination therapies using SP and PD-L1 antibodies for CRC treatment.

Acknowledgements

Not applicable.

Funding

This research was supported by the Natural Science Foundation project of Hubei Province (grant no. 2017CFB571)

and the Health Commission of Hubei Province (grant no. WJ2023F051).

Availability of data and material

The data generated in the present study may be requested from the corresponding author.

Authors' contributions

XW designed and performed the experiments, analysed and interpretated data and wrote the manuscript. YH contributed to the conception and design of the study. XW and YH confirm the authenticity of all the raw data. Both authors have read and approved the final version of the manuscript.

Ethical approval and consent to participate

Not applicable.

Patient consent for publication

Not applicable.

Competing interests

The authors declare that they have no competing interests.

References

1. Siegel RL Giaquinto AN and Jemal A: Cancer statistics, 2024. CA Cancer J Clin 74: 12-49, 2024.
2. Biller LH and Schrag D: Diagnosis and treatment of metastatic colorectal cancer: A review. JAMA 325: 669-685, 2021.
3. Ganesh K, Stadler ZK, Cercek A, Mendelsohn RB, Shia J, Segal NH and Diaz LA Jr: Immunotherapy in colorectal cancer: Rationale, challenges and potential. Nat Rev Gastroenterol Hepatol 16: 361-375, 2019.
4. Yi M, Zheng X, Niu M, Zhu S, Ge H and Wu K: Combination strategies with PD-1/PD-L1 blockade: Current advances and future directions. Mol Cancer 21: 28, 2022.
5. Arifuzzaman M, Collins N, Guo CJ and Artis D: Nutritional regulation of microbiota-derived metabolites: Implications for immunity and inflammation. Immunity 57: 14-27, 2024.
6. Wu H, Mu C, Xu L, Yu K, Shen L and Zhu W: Host-microbiota interaction in intestinal stem cell homeostasis. Gut Microbes 16: 2353399, 2024.
7. Hurst NR, Kendig DM, Murthy KS and Grider JR: The short chain fatty acids, butyrate and propionate, have differential effects on the motility of the guinea pig colon. Neurogastroenterol Motil 26: 1586-1596, 2014.
8. Meyer JH, Cervenka S, Kim MJ, Kreisl WC, Henter ID and Innis RB: Neuroinflammation in psychiatric disorders: PET imaging and promising new targets Lancet Psychiatry 7: 1064-1074, 2020.
9. Morrison DJ and Preston T: Formation of short chain fatty acids by the gut microbiota and their impact on human metabolism. Gut Microbes 7: 189-200, 2016.
10. He J, Zhang P, Shen L, Niu L, Tan Y, Chen L, Zhao Y, Bai L, Hao X, Li X, *et al*: Short-chain fatty acids and their association with signalling pathways in inflammation, glucose and lipid metabolism. Int J Mol Sci 21: 6356, 2020.
11. Filippone A, Casili G, Scuderi SA, Mannino D, Lanza M, Campolo M, Paterniti I, Capra AP, Colarossi C, Bonasera A, *et al*: Sodium propionate contributes to tumor cell growth inhibition through PPAR-γ signaling. Cancers (Basel) 15: 217, 2022.
12. Wong JM, de Souza R, Kendall CW, Emam A and Jenkins DJ: Colonic health: Fermentation and short chain fatty acids. J Clin Gastroenterol 40: 235-243, 2006.
13. Tran NL, Lee IK, Choi J, Kim SH and Oh SJ: Acetate decreases PVR/CD155 expression via PI3K/AKT pathway in cancer cells. BMB Rep 54: 431-436, 2021.
14. Peng Z, Cheng S, Kou Y, Wang Z, Jin R, Hu H, Zhang X, Gong JF, Li J, Lu M, *et al*: The gut microbiome is associated with clinical response to anti-PD-1/PD-L1 immunotherapy in gastrointestinal cancer. Cancer Immunol Res 8: 1251-1261, 2020.
15. Park HS, Han JH, Park JW, Lee DH, Jang KW, Lee M, Heo KS and Myung CS: Sodium propionate exerts anticancer effect in mice bearing breast cancer cell xenograft by regulating JAK2/STAT3/ROS/p38 MAPK signaling. Acta Pharmacol Sin 42: 1311-1323, 2021.
16. Kim K, Kwon O, Ryu TY, Jung CR, Kim J, Min JK, Kim DS, Son MY and Cho HS: Propionate of a microbiota metabolite induces cell apoptosis and cell cycle arrest in lung cancer. Mol Med Rep 20: 1569-1574, 2019.
17. Khalaf K, Hana D, Chou JT, Singh C, Mackiewicz A and Kaczmarek M: Aspects of the tumor microenvironment involved in immune resistance and drug resistance. Front Immunol 12: 656364, 2021.
18. Peng S, Wang R, Zhang X, Ma Y, Zhong L, Li K, Nishiyama A, Arai S, Yano S and Wang W: EGFR-TKI resistance promotes immune escape in lung cancer via increased PD-L1 expression. Mol Cancer 18: 165, 2019.
19. Tsai TF, Lin JF, Lin YC, Chou KY, Chen HE, Ho CY, Chen PC and Hwang TI: Cisplatin contributes to programmed death-ligand 1 expression in bladder cancer through ERK1/2-AP-1 signaling pathway. Biosci Rep 39: BSR20190362, 2019.
20. Fournel L, Wu Z, Stadler N, Damotte D, Lococo F, Boulle G, Ségal-Bendirdjian E, Bobbio A, Icard P, Trédaniel J, *et al*: Cisplatin increases PD-L1 expression and optimizes immune check-point blockade in non-small cell lung cancer. Cancer Lett 464: 5-14, 2019.
21. Livak KJ and Schmittgen TD: Analysis of relative gene expression data using real-time quantitative PCR and the 2(-Delta Delta C(T)) method. Methods 25: 402-408, 2001.
22. Wang X, Wu R, Liu Y, Zhao Y, Bi Z, Yao Y, Liu Q, Shi H, Wang F and Wang Y: m(6)A mRNA methylation controls autophagy and adipogenesis by targeting Atg5 and Atg7. Autophagy 16: 1221-1235, 2020.
23. Peritz T, Zeng F, Kannanayakal TJ, Kilk K, Eiríksdóttir E, Langel U and Eberwine J: Immunoprecipitation of mRNA-protein complexes. Nat Protoc 1: 577-580, 2006.
24. MIto M, Mimura K, Nakajima S, Saito K, Min AKT, Okayama H, Saito M, Momma T, Saze Z, Ohtsuka M, *et al*: Immune escape mechanism behind resistance to anti-PD-1 therapy in gastrointestinal tract metastasis in malignant melanoma patients with multiple metastases. Cancer Immunol Immunother 71: 2293-2300, 2022.
25. Liu J, Chen Z, Li Y, Zhao W, Wu J and Zhang Z: PD-1/PD-L1 checkpoint inhibitors in tumor immunotherapy. Front Pharmacol 12: 731798, 2021.
26. Jiang T, He X, Zhao Z, Zhang X, Wang T and Jia L: RNA m6A reader IGF2BP3 promotes metastasis of triple-negative breast cancer via SLIT2 repression. FASEB J 36: e22618, 2022.
27. Ryu TY, Kim K, Son MY, Min JK, Kim J, Han TS, Kim DS and Cho HS: Downregulation of PRMT1, a histone arginine methyltransferase, by sodium propionate induces cell apoptosis in colon cancer. Oncol Rep 41: 1691-1699, 2019.
28. Lei X, Lei Y, Li JK, Du WX, Li RG, Yang J, Li J, Li F and Tan HB: Immune cells within the tumor microenvironment: Biological functions and roles in cancer immunotherapy. Cancer Lett 470: 126-133, 2020.
29. Wu Q, Jiang L, Li SC, He QJ, Yang B and Cao J: Small molecule inhibitors targeting the PD-1/PD-L1 signaling pathway. Acta Pharmacol Sin 42: 1-9, 2021.
30. Zhang J, Huang D, Saw PE and Song E: Turning cold tumors hot: From molecular mechanisms to clinical applications. Trends Immunol 43: 523-545, 2022.
31. Rameshbabu S, Labadie BW, Argulian A and Patnaik A: Targeting innate immunity in cancer therapy. Vaccines (Basel) 9: 138, 2021.
32. Karin N: Chemokines in the landscape of cancer immunotherapy: How they and their receptors can be used to turn cold tumors into hot ones?. Cancers (Basel) 13: 6317, 2021).
33. Lin KX, Istl AC, Quan D, Skaro A, Tang E and Zheng X: PD-1 and PD-L1 inhibitors in cold colorectal cancer: Challenges and strategies. Cancer Immunol Immunother 72: 3875-3893, 2023.
34. Xiong W, Gao X, Zhang T, Jiang B, Hu MM, Bu X, Gao Y, Zhang LZ, Xiao BL, He C, *et al*: USP8 inhibition reshapes an inflamed tumor microenvironment that potentiates the immunotherapy. Nat Commun 13: 1700, 2022.

35. Cao J and Yan Q: Cancer epigenetics, tumor immunity, and immunotherapy. Trends Cancer 6: 580-592, 2020.
36. An Y and Duan H: The role of m6A RNA methylation in cancer metabolism. Mol Cancer 21: 14, 2022.
37. Sun T, Wu R and Ming L: The role of m6A RNA methylation in cancer. Biomed Pharmacother 112: 108613, 2019.
38. Pan J, Huang T, Deng Z and Zou C: Roles and therapeutic implications of m6A modification in cancer immunotherapy. Front Immunol 14: 1132601, 2023.
39. Chen LJ, Liu HY, Xiao ZY, Qiu T, Zhang D, Zhang LJ, Han FY, Chen GJ, Xu XM and Zhu JH: IGF2BP3 promotes the progression of colorectal cancer and mediates cetuximab resistance by stabilizing EGFR mRNA in an m(6)A-dependent manner. Cell Death Dis 14: 581, 2023.
40. Xu W, Sheng Y, Guo Y, Huang Z, Huang Y, Wen D, Liu CY, Cui L, Yang Y and Du P: Increased IGF2BP3 expression promotes the aggressive phenotypes of colorectal cancer cells in vitro and vivo. J Cell Physiol 234: 18466-18479, 2019.
41. Wan W, Ao X, Chen Q, Yu Y, Ao L, Xing W, Guo W, Wu X, Pu C, Hu X, *et al*: METTL3/IGF2BP3 axis inhibits tumor immune surveillance by upregulating N(6)-methyladenosine modification of PD-L1 mRNA in breast cancer. Mol Cancer 21: 60, 2022.